Vision Research 160 (2019) 52–59

Contents lists available at ScienceDirect

Vision Research

journal homepage: www.elsevier.com/locate/visres

Refractive index redistribution with accommodation based on finite volume-constant age-dependent mechanical modeling

Min-shan Jiang[a,b], Xiao-li Xu[a], Ting Yang[a], Xue-dian Zhang[a], Feng Li[a,*]

[a] Engineering Research Center of Optical Instruments and Systems, Ministry of Education, Shanghai Key Lab of Modern Optical Systems, University of Shanghai for Science and Technology, Shanghai 200093, China

[b] Department of Biomedical Engineering, Florida International University, Miami, FL 33174, USA

ARTICLE INFO

Keywords:
Human lens
GRIN distribution
AVOCADO model
Accommodation

ABSTRACT

The human lens is considered to have a gradient refractive index (GRIN) distribution. The recently developed accommodating volume-constant age-dependent optical (AVOCADO) model can accurately describe the separate GRIN distributions in the axial and radial directions. Our study uses a finite element method to simulate the accommodation process and calculate the GRIN redistribution based on the AVOCADO model for 25-, 35- and 45-year-old lenses. The parameter p describes the steepness of the GRIN profile towards the lens periphery. The results show that axial *p* values increase with age. Under accommodation, the axial *p* value increases, while the radial *p* value decreases. We also use a ray tracing method to evaluate the optical performance of the lens. The aim of this paper is thus to provide an anatomically finite mechanical lens model with separate axial and radial refractive index profiles for a better understanding of accommodation at different ages.

1. Introduction

The human lens has been studied for decades but is still not fully understood, primarily because of the inhomogeneous refractive distribution of the element. The crystalline lens is considered to have a gradient refractive index (GRIN) structure. The GRIN occurs because of the varying distributions and concentrations of lens proteins. A higher index of refraction results from a higher concentration of protein, while a lower index corresponds to a lower concentration of protein. Therefore, the crystalline lens usually has a lower refractive index near its edge than at its center (Bloemendal et al., 2004). The GRIN distribution in the younger lens smoothly increases from the periphery to the nucleus (Goncharov & Chris, 2007). However, in older eyes, the refractive index has a central plateau with a steep gradient at the periphery (Sheil & Goncharov, 2016). According to optical theory, this GRIN structure may help attenuate both monochromatic and chromatic aberrations (Moffat, Atchison, & Pope, 2002a; Navarro, Palos, & González, 2007; Rama, Pérez, Bao, Flores-Arias, & Gómez-Reino, 2005; Shanzuo et al., 2012).

Under accommodation, the GRIN distribution may change with lens geometry deformation. As the axial width of the eye increases, an increased pressure on the lens from the zonule and a convex curvature of the lens surface are imposed to change the overall lens power. A related redistribution in the refractive index of the lens may also occur, which contributes to the alteration in lens power (Cole, 1982). Studies have reported *in vivo* changes in the full lens with accommodation based on magnetic resonance imaging (MRI) (Dubbelman & Van der Heijde, 2001; Khan, Pope, Verkicharla, Suheimat, & Atchison, 2018; Strenk et al., 1999) and optical coherence tomography (Martinez-Enriquez et al., 2016; Martinez-Enriquez, Pérez-Merino, Velasco-Ocana, & Marcos, 2017). The mechanical properties of the lens not only affect shape alterations but also influence the way in which the cells respond to forces of stretching and relaxation (Bahrami, Heidari, & Pierscionek, 2016). To explain the intracapsular accommodation mechanism, Navarro et al. reported that the curvature gradient strongly impacts lens power; this factor is also key in mediating the refractive index distribution of the lens (Navarro & López-Gil, 2017).

Models have been proposed to account for the GRIN structure of the human lens based on iso-dispersive contours. Goncharov and Dainty introduced a wide-field schematic eye model with a GRIN lens, which uses a fourth-order polynomial describing the refractive structure of the lens (Goncharov & Chris, 2007). Díaz et al. used a combination of polynomials and trigonometric functions for describing the refractive index distribution (Díaz, Pizarro, & Arasa, 2008). Bahrami et al. suggested a monochromatic geometry-invariant GRIN lens (GIGL) model, presenting expressions for the equivalent refractive index and the equivalent Abbe number of the homogeneous equivalent lens (Bahrami & Goncharov, 2012a, 2012b). Navarro et al. proposed a general

* Corresponding author.
E-mail address: lifenggold@163.com (F. Li).

https://doi.org/10.1016/j.visres.2019.04.008
Received 18 December 2018; Received in revised form 29 March 2019; Accepted 5 April 2019
Available online 21 May 2019

schematic model of the optical system of the emmetropic human eye that is capable of adapting to changes with age and accommodation through the adjustment of the optical surfaces and the internal gradient index structure of the lens (Navarro, 2014). As the adjustable internal structure (AIS) with separate axial and radial refractive index profiles was not available with these existing models (Bahrami, Goncharov, & Pierscionek, 2014), a new accommodating volume-constant age-dependent optical (AVOCADO) model was developed by Sheil and Goncharov (2016) The AVOCADO model is age related and has independent axial and radial GRIN distributions that allow decoupling of the axial optical path length. One particularly common simplification is that the iso-indicial surfaces of the GRIN structure are concentric, but the AVOCADO considers two independent axial and radial GRIN distributions, and hence, the iso-indicial surfaces are not necessarily concentric, which is more realistic. This novel model is selected for our study.

To investigate the redistribution of the refractive index with accommodation, Bahrami et al. used an axial-reduced accommodation model to connect the inhomogeneous mechanical characteristics of the lens to the optical performance (Bahrami et al., 2016). As an improvement in the reduced model for only the younger lens, in this article, we propose a finite element model based on the AVOCADO method to present crystalline lens contours and the refractive index distribution under accommodation. With this improved model, we can further understand the mechanical properties and the accommodation status of the lens at different ages.

2. Method

2.1. GRIN lens contours

For modeling the lens *in vitro*, the coordinates of the GRIN profile are divided along the equator into anterior and posterior sections. Both the normalized axial and radial refractive indexes of the crystalline lens can be calculated by a power function (Bahrami & Goncharov, 2012a; Smith, Atchison, & Pierscionek, 1992):

$$n(\zeta) = n_c + (n_s - n_c)(\zeta^2)^p \tag{1}$$

where n_c is the refractive index at the center and n_s is the refractive index at the surface of the GRIN lens. ζ is the normalized distance from the center. The value of ζ ranges from -1 to $+1$, corresponding to the range from the anterior to the posterior surface of the lens. ζ^2 is introduced to prevent complex results. The parameter p describes the steepness of the refractive index profile towards the lens periphery, it accounts for some optically significant age-related changes in the GRIN structure. When p increases, the central flat portion of the index distribution also increases.

The AVOCADO model is accurate for presenting age-related bulk changes in the GRIN (Sheil & Goncharov, 2016). In this model, the radii are scaled nonlinearly according to an appropriate power m of ζ. The internal contour height is expressed as follows:

$$\rho^2 = 2\zeta^{2m+1}R_a(\zeta T_a + z) - \zeta^{2m}(1 + K_a)(\zeta T_a + z)^2 + \zeta^{2m-1}B_a(\zeta T_a + z)^3 \tag{2}$$

where R_a and K_a are the radius and the conic constant, respectively, of the anterior surface. T_a is the thickness from the nucleus to the pole of the anterior portion. m is the age-related parameter, shown as follows (Sheil & Goncharov, 2017):

$$m = 0.6 - \left(\frac{A}{90}\right)^4 \tag{3}$$

where A is the age. In addition, the corresponding p can be calculated by the following equation:

$$p = 2.85 + 0.5\left(\frac{A}{46}\right)^4 \tag{4}$$

As an improvement to the GIGL model (Bahrami & Goncharov, 2012a), the AVOCADO model treats the refractive index as decreasing radially from the nucleus to the surface along the line $z = 0$ by the exponent $2p/(m + 1)$. With the exponents $2p$ and $2p/(m + 1)$, the axial and radial GRIN profiles in the AVOCADO model can be decoupled from the age-related parameter, and the corresponding index distributions are independent.

The iso-indicial contours of lenses modeled at different ages are shown in Fig. 1. R_p and K_p are the radius and the conic constant, respectively, of the posterior surface. T_p is the thickness from the nucleus to the pole of the posterior portion. The conic constant of the lens contours does not obviously influence the power of the lens (Tabernero,

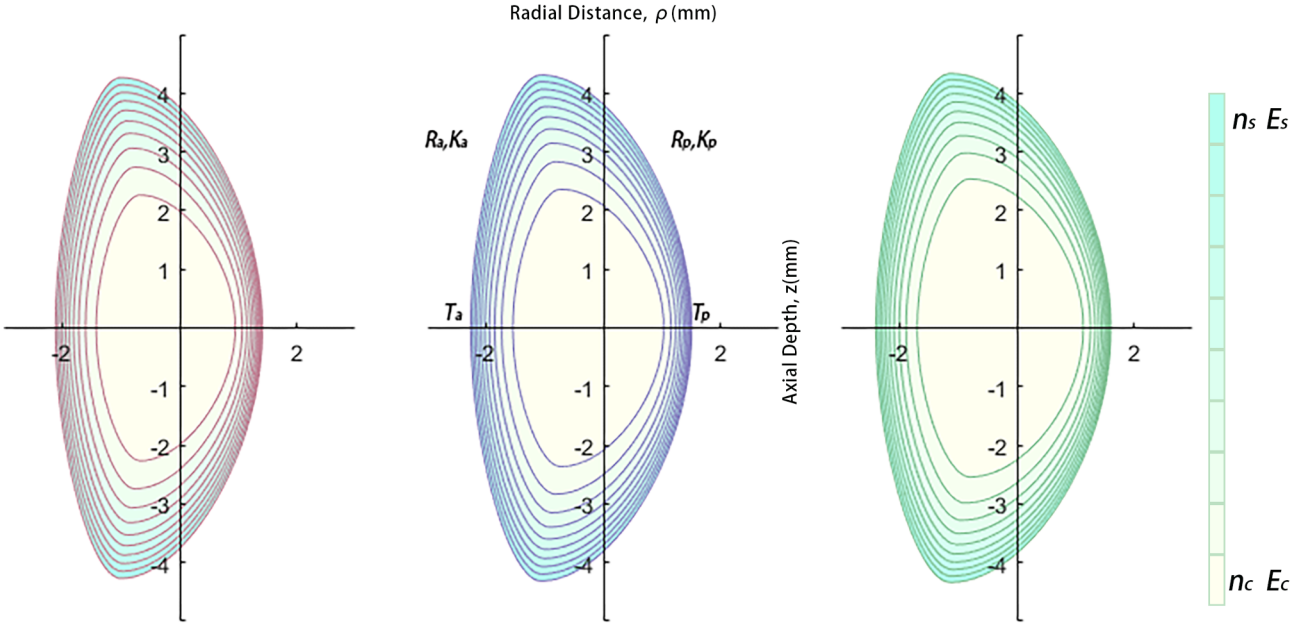

Fig. 1. Iso-indicial shells modeled at different ages. (a) 25 years old, (b) 35 years old, and (c) 45 years old. $T_a = 0.6 \times (2.93 + 0.024A)$, $T_p = 0.4 \times (2.93 + 0.024A)$, $R_a = 12.7–0.057A$, $R_p = 5.9–0.012A$. The z axis ($\rho = 0$) presents the axial direction. The ρ axis ($z = 0$) presents the radial direction. The legend shows the distribution of Young's modulus and refractive index in the model.

Berrio, & Artal, 2011), but the spherical aberration (SA) has a strong correlation with the conic constant. We use the conic constant $K_a = -4.5 + 0.03/\text{yr}$ and $K_p = -1.1 + 0.02/\text{yr}$. Fig. 1 shows ten iso-indicial contours with uniform refractive index variation. To preserve the optical integrity of the GRIN structure of the lens, the number of contours does not change with accommodation.

2.2. Finite element model

When viewing a near object, the circularly arranged ciliary muscle contracts, allowing the lens zonule and suspensory ligaments to press on the lens. The source of the tension is the pressure that the vitreous and aqueous humors exert outward force on the sclera (Baumeister & Kohnen, 2008). According to Newton's 3rd law of motion, the force on both sides of these springs in series is identical to the force applied at the poles of the lens when the lens shape changes (Bahrami et al., 2016). The radial displacement δr can be expressed following Hooke's law:

$$\delta r = \frac{F}{k_r} = \frac{Fr}{S_0 E_r} \tag{5}$$

where F is the force applied to the contact boundary of the lens. k_r and E_r are the spring constant and Young's modulus of individual layers, respectively. S_0 is the force-applied area. r is the initial radial length of a small spring.

To perform the mechanical finite analysis of the age-related changes in the crystalline lens of the eye, we used the COMSOL Multiphysics software (Comsol Inc., MA, USA, version 5.3a). We calculated the coordinates of the shells with MATLAB (MathWorks Inc., MA, USA, version R2018a) and then imported the parameterized curves into COMSOL. The cross-section of the mesh geometry model includes 10 iso-indicial shells (35-year-old lens), both capsular and zonular, as shown in Fig. 2. The lower right corner of the figure is a diagram of the human eye structure. Due to the symmetry of the lens, the cross-section (the red part) of the rotationally symmetric meshed geometry was used for finite modeling. The anterior and posterior surfaces correspond to the upper and lower boundaries, respectively. To simulate the crystalline lens, the model is rotationally symmetric around the axis $\rho = 0$. To improve the calculation accuracy, the maximum grid unit was defined as approximately 0.02 mm. The total number of cross-sectional meshgrid elements is 39,463 for the 25-year-old lens, 42,489 for the 35-year-old lens and 46,361 for the 45-year-old lens. The thickness of the capsule varies from 0.01 mm at the poles to 0.02 mm at the equator (Bahrami et al., 2016; Forrester, Dick, Mcmenamin, & Roberts, 2007).

Table 1
Young's modulus and refractive index in the finite element model (Fisher, 1969, 1971; Moffat et al., 2002b).

Age (yr)	E_c (Pa)	E_s (Pa)	$E_{capsular}$ (MPa)	n_c	n_s
25	521	3158	5.2	1.4315	1.3643
35	642	3657	5.0	1.4281	1.3640
45	997	3976	4.5	1.4247	1.3637

As the zonule of Zinn is a ring of fibrous strands connecting the ciliary body to the lens and is difficult to visualize, this structure is simply modeled as a single trapeze entity contacting the capsular region. Although the zonular-free zone diameter tends to decrease with age, the differences in the diameter of this zone in different age groups can be ignored (Lim et al., 1998).

To build an accurate model, we used different Young's moduli according to different ages, as shown in Table 1 (Fisher, 1969, 1971). E_c and E_s are Young's moduli of the center and the surface, respectively. The stiffness of both the lenticular nucleus and the periphery increases with age but at different rates (Weeber, Eckert, Pechhold, & van der Heijde, 2007). By contrast, the elasticity of the lens capsule decreases with age, which is presumably a cause of presbyopia (Fisher, 1969, 1971). The cross-section of the zonule is represented by a Young's modulus of 10^7 Pa (Michael et al., 2012).

The refractive index values used for both the center (n_c) and the surface (n_s) are also shown in Table 1 (Moffat, Atchison, & Pope, 2002b). Both n_c and n_s decrease with age. The decline in the nuclear refractive index coincides with numerous changes in the crystallin proteins of the lens. Our model is divided into 10 shells with equal increments in the magnitude of the refractive index from the center to the surface (Moffat et al., 2002b). The Poisson ratios are set at 0.49 for the lens material and 0.47 for the lens capsule (Bahrami et al., 2016).

3. Results

3.1. Mechanical analysis

To stimulate a similar range of accommodation, a displacement of −0.15 mm in the radial directions was applied to the contact boundary of the lens. The principal strain distributions for 25-, 35- and 45-year-old lenses are shown in Fig. 3. The contour change is obviously more marked in the central region under accommodation. The boundary of the central region can be clearly observed in the figures corresponding to higher

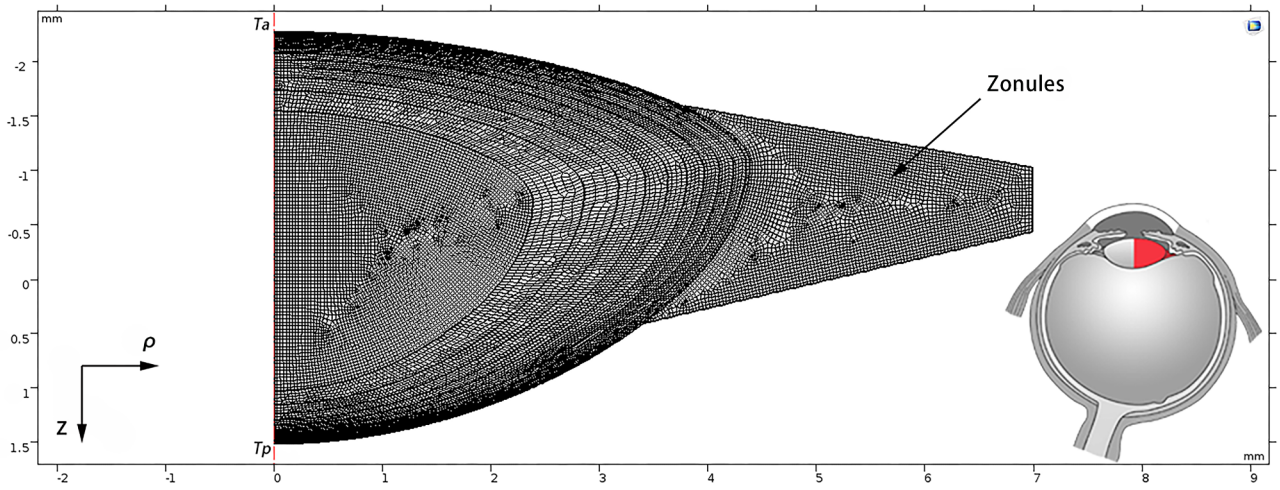

Fig. 2. Cross-section of the lens (the red part of the eye diagram in the lower right corner) with iso-indicial shells and mesh grids for a 35-year-old lens. $\rho = 0$ (the dashed red line) represents the axis of symmetry. (For interpretation of the references to colour in this figure legend, the reader is referred to the web version of this article.)

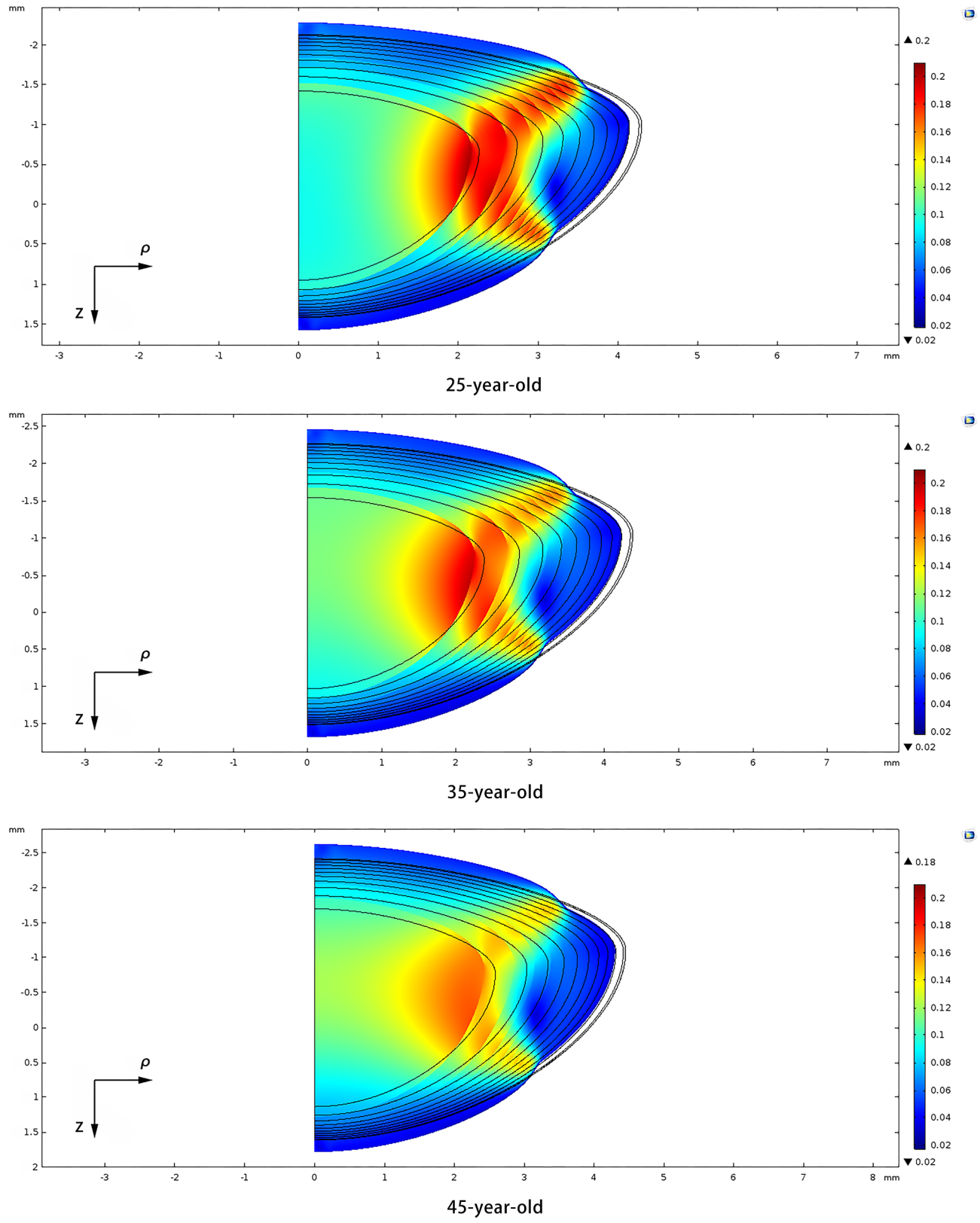

Fig. 3. The deformation of the lens with a −0.15 mm radial displacement. The legend shows the equivalent elastic strain values.

levels of strain. Compared with the center, the strain of the outer layers, especially the polar regions, is very low. The strain distribution around the poles increases noticeably from the surface layer to the nuclear layer. The high strain is mainly distributed in the equatorial region of the inner layers and shows a bifurcation that extends to the surface.

The optical parameters of 25-, 35- and 45-year-old lenses (axial thickness, radius of curvature, conic constant, and volume) with/without accommodation are shown in Table 2. At all ages, the axial thickness of the lens increases with accommodation. In our simulation, the lenses of different ages have different volumes, and the volume of

Table 2
The optical parameters of 25-, 35- and 45-year-old lenses with/without accommodation.

Age (yr)	Accommodation status	T (mm)	R_a (mm)	R_p (mm)	K_a	K_p	V (mm^3)
25	Accommodated	3.84	7.03	4.97	−7.32	−1.39	137.81
	Unaccommodated	3.53	11.28	5.60	−4.50	−1.10	137.81
35	Accommodated	4.13	6.26	4.87	−8.11	−1.10	151.91
	Unaccommodated	3.77	10.71	5.48	−4.20	−0.90	151.91
45	Accommodated	4.39	5.77	4.75	−8.22	−0.78	165.59
	Unaccommodated	4.01	10.14	5.36	−3.90	−0.70	165.59

the lens is considered constant with accommodation. The volume can be calculated using the following equation (Sheil, Bahrami, & Goncharov, 2014):

$$V = \frac{\pi}{6}\left[5R_pZ_p^2 + 5R_aZ_a^2 - Q_pZ_p^3 - Q_aZ_a^3\right] \quad (6)$$

where V is the volume of the lens. Q_a and Q_p are the shape factor of the anterior and posterior surfaces of the lens, respectively, and are given by $Q = 1 + K$. Supposing that Z_c is the axial position of the lens equator, the anterior and posterior axial thicknesses of the lens are given by $Z_a = T_a + Z_c$ and $Z_p = T_p - Z_c$, respectively.

3.2. Refractive index distribution

The deformation of the crystalline lens causes the redistribution of the refractive index. Different shells present different indexes. The coordinates of each shell were extracted from Fig. 3. The axial width of each layer clearly expands because of accommodation. The axial thickness of the inner layers increases more than that of the outer layers, and the maximum increase in the axial thickness is observed in the innermost layer, mainly because the Young's modulus is lower in the core and higher on the surface (Table 1). The expansion of the contours causes the increase in the width of the refractive index distribution. The distributions of the axial index profiles under accommodation at different ages are shown in Fig. 4 as blue dashed-dotted lines; the profile flattens with accommodation. The unaccommodated distributions are shown as orange solid lines. From these figures, it is clear that the axial refractive index profiles flatten in the central region with accommodation. Accordingly, the widths of the radial refractive index profiles become narrow.

The p value was calculated in MATLAB to fit power law curves to the points via the curve fitting method. Without accommodation, the axial p values fitted from the curve are consistent with those calculated from Eq. (4). Tables 3(a) and (b) show the axial and radial p values at different ages, respectively, as calculated with our finite element model. Consistent with the description of the AVOCADO model, the axial and radial GRIN profiles are independent. The radial exponent is $2/(m + 1)$ to the axial p value when the ciliary muscle is relaxed. Accordingly, under accommodation, the axial p value increases by 0.2, while the radial p value decreases. In addition, the axial p values for both accommodation and unaccommodation increase with age; this result is consistent with that calculated with Eq. (4).

3.3. Optical power and spherical aberration

The small difference between the exponential coefficients of the profiles may affect optical and imaging performance. Tables 4 and 5 present the optical power and the SA, respectively, as calculated by the paraxial ray tracing method from the axial p value (Table 3(a)) (Bahrami & Goncharov, 2012a; Sheil et al., 2014). The pupil is located at the anterior surface of the lens, and the diameter is set as 3 mm. The refractive index of the medium surrounding the lens is 1.336.

As shown in Tables 4 and 5, with the increase in the axial p value under accommodation, the optical power increases. For the AVOCADO model, as shown in Eq. (3), the growth with age results in a decrease in m. Therefore, although the difference in the axial p value between the accommodated and unaccommodated states remains relatively constant for different age groups, the exact difference in the optical power increases with age.

Our model also shows that the small difference in the axial p value between the accommodated and unaccommodated states results in greater differences in SA. In the paraxial ray tracing method, the radial p value is not considered to critically influence the results since the refractive index of the core is a smooth function of ζ. As a result, the optical performance stabilizes when the pupil diameter is limited in the core region. Otherwise, with an additional parameter related to m introduced into the AVOCADO model, we can easily decouple SA and optical power using the separated p values.

4. Discussion and conclusion

In our study, the finite mechanical model simulated accommodation with a zonule displacement of −0.15 mm. This accommodation changes the equatorial diameter by 0.3 mm. Because of the volume growth with ages, the same level of accommodation changes the lens thickness by 0.31 mm at age 25 years and by 0.38 mm at age 45 years. Dubbelman et al. found a mean change in the lens thickness of 0.045 ± 0.012 mm/D, and the change in thickness per diopter was not significantly dependent on the anterior or posterior lens radius or the curvature (Dubbelman, Van der Heijde, & Weeber, 2005). Thus, a mean lens thickness change in 0.36 mm with a range from 0.26 to 0.46 mm is expected under the accommodation of 8D, which is consistent with our results. Khan et al. investigated changes in lens dimensions with accommodation using a 3 T clinical MRI scanner (Khan et al., 2018). In Khan's study, when the lens equatorial diameter decreased by 0.30 mm (from a mean value of 9.29 mm to 8.99 mm) under accommodation, the total axial lens thickness increased by 0.34 mm (from a mean value of 3.55 mm to 3.89 mm). As Khan's study used 18- to 29-year-old patients, these clinical results for changes in the lens thickness agree with our simulated results.

The principal strain distribution of our mechanical model is mainly affected by Young's modulus. The data on Young's modulus used in our paper were obtained by Fisher in 1971 from human cadavers not more than 24 h after death (Fisher, 1971). A continuous increase in Young's modulus of cortical elasticity has been observed until approximately 50 years of age. This increase is presumed to be caused by a senile shift in the proportion of long- to short-chain protein molecules within the cortical lens fibers and reduces the maximum value of the principal strain under the same level of accommodation. In our study, we investigated the model for lenses of ages 25, 35 and 45 years. Throughout these years, the stiffness of both the lenticular nucleus and the periphery mainly increases with age but at different rates (Weeber et al., 2007). The nuclear values increase more rapidly than those of the cortex; in lenses over the age of 50, the stiffness of the lens nucleus was

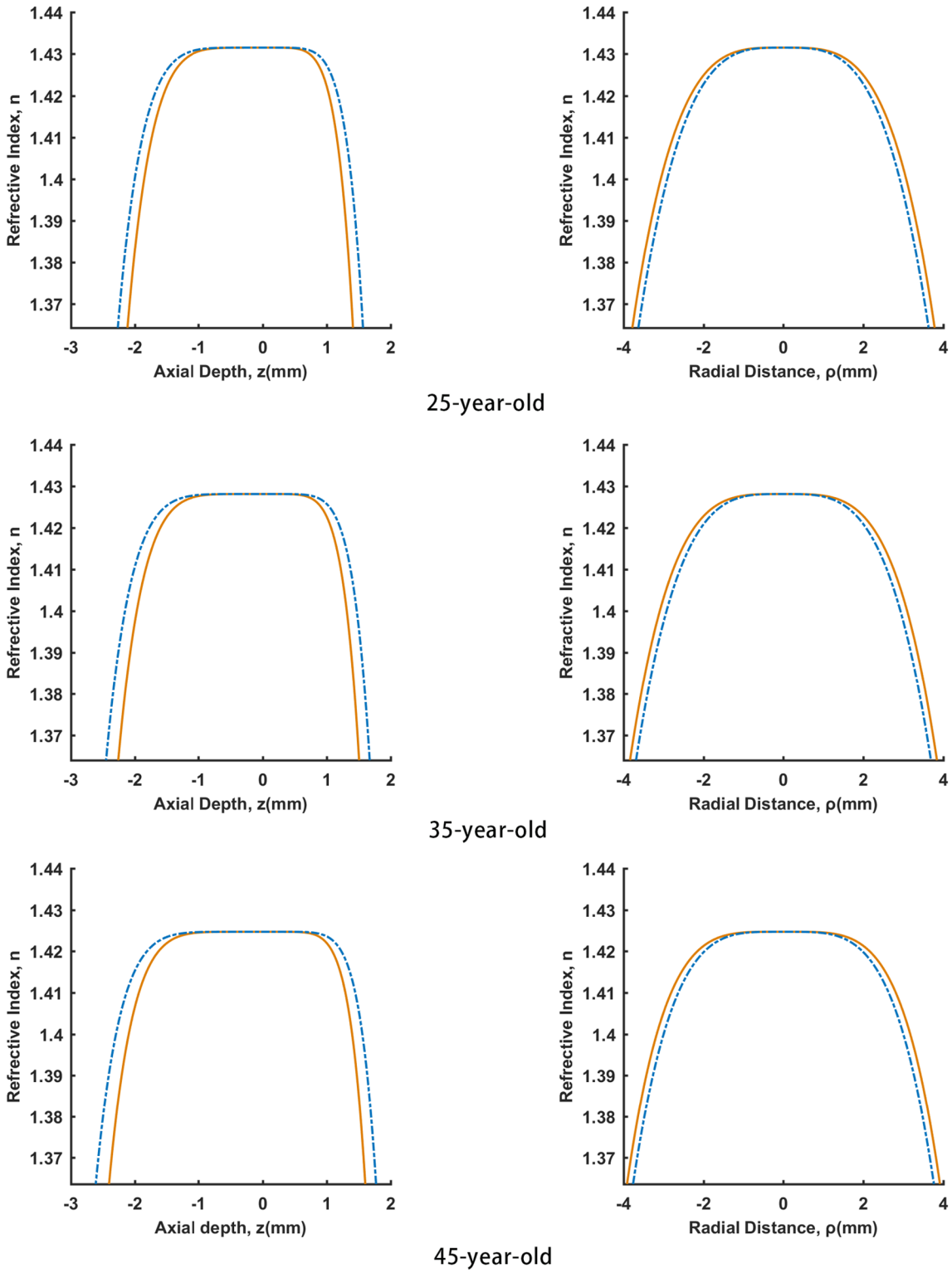

Fig. 4. Refractive index distribution profiles in two directions with a −0.15 mm displacement. Left panel: axial direction; right panel: radial direction. Blue dashed-dotted line: accommodated. Orange solid line: unaccommodated. (For interpretation of the references to colour in this figure legend, the reader is referred to the web version of this article.)

typically an order of magnitude greater than that of the cortex (Heys, Cram, & Truscott, 2004). For older human eyes, no significant correlation exists between Young's modulus and age (Michael et al., 2012).

With the displacement of the zonule in our finite model, the geometrical change is greater in the polar regions of the inner layers than in the same region of the outer layers. The widening of the central part with simulated accommodation is consistent with early clinical reports of a widening of the nuclear region under accommodation. As a result of contour deformation under accommodation, the lens GRIN profiles change. The anterior and posterior axial refractive index profiles steepen at the periphery, while the radial refractive index profiles flatten, which agrees with the MRI results (Khan et al., 2018). These

Table 3
p value with/without accommodation at different ages.

(a) Axial				(b) Radial			
Accommodation status	Age (yr)			Accommodation status	Age (yr)		
	25	35	45		25	35	45
Accommodated	3.07	3.21	3.51	Accommodated	1.72	1.78	1.99
Unaccommodated	2.89	3.01	3.3	Unaccommodated	1.82	1.91	2.15

Table 4
Optical powers (D) with/without accommodation at different axial p values.

Accommodation status	Age (yr)		
	25	35	45
Accommodated	36.752495	34.636053	32.829245
Unaccommodated	28.932826	26.639694	24.75598

Table 5
Spherical aberrations (μm) with/without accommodation at different axial p values.

Accommodation status	Age (yr)		
	25	35	45
Accommodated	−0.666	−1.184875	−1.398625
Unaccommodated	0.129375	0.139125	0.139875

GRIN profile redistributions increase the *p* values for the axial profiles and decrease the *p* values for the radial profiles. These trends are consistent across all age groups.

Nevertheless, our study has limitations. First, although Dubbelman et al. found that the change in thickness per diopter with age is not significant (Dubbelman et al., 2005), and the applied displacement of −0.15 mm does not exactly correspond to an 8D accommodation at all ages. Second, the stimulation of the zonule is approximate because the zonular insertions are not precisely known. In contrast with the classical description, recent anatomical studies show new insertions of the zonule. Bernal et al. found that the majority of the posterior zonular fibers are not attached directly to the posterior lens capsule but anchored to the anterior hyaloid membrane on their path from the ciliary body to the posterior capsule (Bernal, Parel, & Manns, 2006). Nankivil found that either the anterior or posterior zonules alone can change the shape of both lens surfaces under accommodation. The anterior zonules have a greater effect on the anterior lens surface, and the posterior zonules have a greater effect on the posterior lens surface (Nankivil et al., 2015). Wang et al.'s model showed that the anterior and posterior zonules may have a greater impact on changes in shape than the equatorial zonules (Wang, Venetsanos, Wang, & Pierscionek, 2016; Wang, Venetsanos, Wang, Augousti, & Pierscionek, 2017). Therefore, further investigation is needed to determine how the zonule affects the accommodation status.

To the best of our knowledge, this study is the first to use a finite element model to simulate the GRIN structures with the AVOCADO method and analyze the GRIN distributions with accommodation in both the axial and radial directions at different lens ages. In addition, optical powers and SA are calculated for further discussion. The aim of our future work is to develop an anatomically accurate model characterizing the geometrical structure, optical performance and biomechanical properties of the aging lens. We hope that this study will be helpful for modeling a physically realistic lens using ray tracing software and will provide a better understanding of the accommodation process.

Acknowledgments

This research was supported by Exploring Scientific Instrument of China (2013YQ03065104), the National Science Technology Major Project of the Ministry of Science and Technology of China (2014ZX07104).

Appendix A. . A list of symbols and abbreviations

Symbols:	
A	age
E	Young's modulus
K	conic constant
n_c	refractive index at the center
n_s	refractive index at the surface
Q	shape factor of the lens
R	radius of the lens
T	thickness of the lens
V	volume of the lens
ζ	normalized distance from the center
Abbreviations:	
AVOCADO	Accommodating volume-constant age-dependent optical
GIGL	Geometry-invariant gradient refractive index lens
GRIN	Gradient refractive index
MRI	Magnetic resonance imaging
SA	Spherical aberration

References

Bahrami, M., & Goncharov, A. V. (2012a). Geometry-invariant gradient refractive index lens: Analytical ray tracing. *Journal of Biomedial Optics, 17*(5), 055001. https://doi.org/10.1117/1.JBO.17.5.055001.

Bahrami, M., & Goncharov, A. V. (2012b). Geometry-invariant GRIN lens: Iso-dispersive contours. *Biomedical Optics Express, 3*(7), 1684–1700. https://doi.org/10.1364/BOE.3.001684.

Bahrami, M., Goncharov, A. V., & Pierscionek, B. K. (2014). Adjustable internal structure for reconstructing gradient index profile of crystalline lens. *Optics Letters, 39*(5), 1310–1313. https://doi.org/10.1364/OL.39.001310.

Bahrami, M., Heidari, A., & Pierscionek, B. K. (2016). Alteration in refractive index profile during accommodation based on mechanical modelling. *Biomedical Optics Express, 7*(1), 99–110. https://doi.org/10.1364/BOE.7.000099.

Baumeister, M., & Kohnen, T. (2008). [Accommodation and presbyopia: Part 1: Physiology of accommodation and development of. *presbyopia]. 105*(6), 597.

Bernal, A., Parel, J. M., & Manns, F. (2006). Evidence for posterior zonular fiber attachment on the anterior hyaloid membrane. *Investigative Ophthalmology & Visual Science, 47*(11), 4708–4713. https://doi.org/10.1167/iovs.06-0441.

Bloemendal, H., de Jong, W., Jaenicke, R., Lubsen, N. H., Slingsby, C., & Tardieu, A. (2004). Ageing and vision: Structure, stability and function of lens crystallins. *Progress in Biophysics and Molecular Biology, 86*(3), 407–485. https://doi.org/10.1016/j.pbiomolbio.2003.11.012.

Cole, D. F. (1982). Adler's physiology of the eye: Clinical application. *The British Journal of Ophthalmology, 66*(11) 743–743.

Díaz, J. A., Pizarro, C., & Arasa, J. (2008). Single dispersive gradient-index profile for the aging human lens. *Journal of the Optical Society of America A, 25*(1), 250–261. https://doi.org/10.1364/JOSAA.25.000250.

Dubbelman, M., & Van der Heijde, G. L. (2001). The shape of the aging human lens: Curvature, equivalent refractive index and the lens paradox. *Vision Research, 41*(14), 1867–1877. https://doi.org/10.1016/S0042-6989(01)00057-8.

Dubbelman, M., Van der Heijde, G. L., & Weeber, H. A. (2005). Change in shape of the aging human crystalline lens with accommodation. *Vision Research, 45*(1), 117–132. https://doi.org/10.1016/j.visres.2004.07.032.

Fisher, R. F. (1969). Elastic constants of the human lens capsule. *Journal of Physiology, 201*(1), 1–19.

Fisher, R. F. (1971). The elastic constants of the human lens. *Journal of Physiology, 212*(1), 147–180.

Forrester, J. V., Dick, A. D., Mcmenamin, P. G., & Roberts, F. (2007). *The eye: Basic sciences in practice.* Saunders.

Goncharov, A. V., & Chris, D. (2007). Wide-field schematic eye models with gradient-index lens. *Journal of the Optical Society of America A, 24*(8), 2157–2174.

Heys, K. R., Cram, S. L., & Truscott, R. J. (2004). Massive increase in the stiffness of the human lens nucleus with age: The basis for presbyopia? *Molecular Vision, 10*(10), 956–963.

Khan, A., Pope, J. M., Verkicharla, P. K., Suheimat, M., & Atchison, D. A. (2018). Change in human lens dimensions, lens refractive index distribution and ciliary body ring diameter with accommodation. *Biomedical Optics Express, 9*(3), https://doi.org/10.1364/boe.9.001272.

Lim, S. J., Kang, S. J., Kim, H. B., Kurata, Y., Sakabe, I., & Apple, D. J. (1998). Analysis of zonular-free zone and lens size in relation to vial length of eye with age. *Journal of Cataract & Refractive Surgery, 24*(3), 390–396. https://doi.org/10.1016/s0886-3350(98)80329-5.

Martinez-Enriquez, E., Pérez-Merino, P., Velasco-Ocana, M., & Marcos, S. (2017). OCT-based full crystalline lens shape change during accommodation in vivo. *Biomedical Optics Express, 8*(2), 918–933. https://doi.org/10.1364/BOE.8.000918.

Martinez-Enriquez, E., Sun, M., Velasco-Ocana, M., Birkenfeld, J., Perez-Merino, P., & Marcos, S. (2016). Optical coherence tomography based estimates of crystalline lens volume, equatorial diameter, and plane position. *Investigative Ophthalmology & Visual Science, 57*(9), OCT600-610. https://doi.org/10.1167/iovs.15-18933.

Michael, R., Mikielewicz, M., Gordillo, C., Montenegro, G. A., Pinilla Cortes, L., & Barraquer, R. I. (2012). Elastic properties of human lens zonules as a function of age in presbyopes. *Investigative Ophthalmology & Visual Science, 53*(10), 6109–6114. https://doi.org/10.1167/iovs.11-8702.

Moffat, B. A., Atchison, D. A., & Pope, J. M. (2002a). Age-related changes in refractive index distribution and power of the human lens as measured by magnetic resonance micro-imaging in vitro. *Vision Research, 42*(13), 1683–1693. https://doi.org/10.1016/s0042-6989(02)00078-0.

Moffat, B. A., Atchison, D. A., & Pope, J. M. (2002b). Explanation of the lens paradox. *Optometry and Vision Science, 79*(3), 148–150. https://doi.org/10.1097/00006324-200203000-00008.

Nankivil, D., Maceo Heilman, B., Durkee, H., Manns, F., Ehrmann, K., Kelly, S., ... Parel, J. M. (2015). The zonules selectively alter the shape of the lens during accommodation based on the location of their anchorage points. *Investigative Ophthalmology & Visual Science, 56*(3), 1751–1760. https://doi.org/10.1167/iovs.14-16082.

Navarro, R. (2014). Adaptive model of the aging emmetropic eye and its changes with accommodation. *Journal of Visualized Experiments, 14*(13), 21. https://doi.org/10.1167/14.13.21.

Navarro, R., & López-Gil, N. (2017). Impact of internal curvature gradient on the power and accommodation of the crystalline lens. *Optica, 4*(3), https://doi.org/10.1364/optica.4.000334.

Navarro, R., Palos, F., & González, L. (2007). Adaptive model of the gradient index of the human lens. I. Formulation and model of aging ex vivo lenses. *Journal of the Optical Society of America A, 24*(8), 2175–2185. https://doi.org/10.1364/JOSAA.24.002175.

Rama, M.a. A., Pérez, M.a. V., Bao, C., Flores-Arias, M.a. T., & Gómez-Reino, C. (2005). Gradient-index crystalline lens model: A new method for determining the paraxial properties by the axial and field rays. *Optics Communications, 249*(4–6), 595–609. https://doi.org/10.1016/j.optcom.2005.01.035.

Shanzuo, J., Michael, P., Lepkowicz, R. S., Armand, R., Richard, F., Guy, B., & Eric, B. (2012). A bio-inspired polymeric gradient refractive index (GRIN) human eye lens. *Optics Express, 20*(24), 26746–26754.

Sheil, C. J., Bahrami, M., & Goncharov, A. V. (2014). An analytical method for predicting the geometrical and optical properties of the human lens under accommodation. *Biomedical Optics Express, 5*(5), 1649–1663. https://doi.org/10.1364/BOE.5.001649.

Sheil, C. J., & Goncharov, A. V. (2016). Accommodating volume-constant age-dependent optical (AVOCADO) model of the crystalline GRIN lens. *Biomedical Optics Express, 7*(5), 1985–1999. https://doi.org/10.1364/BOE.7.001985.

Sheil, C. J., & Goncharov, A. V. (2017). Crystalline lens paradoxes revisited: Significance of age-related restructuring of the GRIN. *Biomedical Optics Express, 8*(9), 4172–4180. https://doi.org/10.1364/BOE.8.004172.

Smith, G., Atchison, D. A., & Pierscionek, B. K. (1992). Modeling the power of the aging human eye. *Journal of the Optical Society of America A, 9*(12), 2111–2117. https://doi.org/10.1364/JOSAA.9.002111.

Strenk, S. A., Semmlow, J. L., Strenk, L. M., Munoz, P., Gronlund-Jacob, J., & DeMarco, J. K. (1999). Age-related changes in human ciliary muscle and lens: A magnetic resonance imaging study. *Investigative Ophthalmology & Visual Science, 40*(6), 1162–1169.

Tabernero, J., Berrio, E., & Artal, P. (2011). Modeling the mechanism of compensation of aberrations in the human eye for accommodation and aging. *Journal of the Optical Society of America A, 28*(9), 1889–1895. https://doi.org/10.1364/JOSAA.28.001889.

Wang, K., Venetsanos, D. T., Wang, J., Augousti, A. T., & Pierscionek, B. K. (2017). The importance of parameter choice in modelling dynamics of the eye lens. *Scientific Reports, 7*(1), 16688. https://doi.org/10.1038/s41598-017-16854-9.

Wang, K., Venetsanos, D., Wang, J., & Pierscionek, B. K. (2016). Gradient moduli lens models: How material properties and application of forces can affect deformation and distributions of stress. *Scientific Reports, 6*, 31171. https://doi.org/10.1038/srep31171.

Weeber, H. A., Eckert, G., Pechhold, W., & van der Heijde, R. G. (2007). Stiffness gradient in the crystalline lens. *Graefes Archive for Clinical and Experimental Ophthalmology, 245*(9), 1357–1366. https://doi.org/10.1007/s00417-007-0537-1.